# Motion Dynamics and Control of a Planetary Rover With Slip-Based Traction Model

Kazuya Yoshida and Hiroshi Hamano

Tohoku University, Aoba 01, Sendai, Japan

## ABSTRACT

This paper investigates kinetic behavior of a planetary rover with attention to tire-soil traction mechanics and articulated body dynamics, and thereby study the control when the rover travels over natural rough terrain. Experiments are carried out with a rover test bed to observe the physical phenomena of soils and to model the traction mechanics, using the tire slip ratio as a state variable. The relationship of load-traction factor versus the slip ratio is modeled theoretically then verified by experiments, as well as specific parameters to characterize the soil are identified. A dynamic simulation model is developed considering the characteristics of wheel actuators, the mechanics of tire-soil traction, and the articulated body dynamics of a suspension mechanism. Simulations are carried out to be compared with the corresponding experimental data and verified to represent the physical behavior of a rover. Finally, a control method is proposed and tested. The proposed method keeps the slip ratio within a small value and limits excessive tire force, so that the rover can successfully traverse over the obstacle without digging the soil or being stuck.

**Keywords:** planetary exploration, rover test bed, tire-soil mechanics, load traction factor, slip ratio, articulated body dynamics

## 1. INTRODUCTION

The effectiveness of a surface locomotion rover in planetary exploration has been proven by NASA's Pathfinder mission in 1997[1] and, in upcoming missions, rovers are expected to traverse much longer distance over more challenging terrain, then achieve more complex tasks.

Corresponding to such growing attention, there are an increasing number of research papers being published to deal with technological issues on exploration rovers. The research area is very broad from mission design and analysis,[34] rover designs,[567] sensing and navigation, obstacle avoidance, path planning,[8] motion kinematics and slip model,[9] field test,[1011] and so on. However, very few have dealt with motion dynamics of rovers yet. This is because the rovers are, so far, considered to move too slowly to experience dynamic effect, and also the dynamic analysis requires complicated models and computation.

But recently, some papers report advantage of physics based motion control that involves a model of traction mechanics with the consideration of force distribution among the wheels.[12131415] In this approach the wheel-soil contact angle and the distribution of the load on each wheel were discussed, then an optimum control law that maximizes the traction and minimizes the power consumption was derived.[915] In these papers, ground contact and force analysis were highlighted.

Extending the above approach, in the present paper, we investigate the tire-soil traction mechanics as well as the body-suspension-wheel dynamics of a rover. From the mission aspect, an exploration rover is discussed in Japan for a possible un-manned mission to the Moon,[16] which will be jointly managed by NASDA (National Space Development Agency of Japan), ISAS (Institute of Space and Astronautical Science, Japan) and NAL (National Aerospace Laboratory of Japan.) On the lunar surface, terrain is composed mostly by fine grained soil (regolith) in which a rover may be easily stuck, and the gravity is smaller then a rover bounces more dynamically.

Further author information: (Send correspondence to Dr. Kazuya Yoshida)
Kazuya Yoshida: E-mail: yoshida@astro.mech.tohoku.ac.jp, Telephone: +81 (0)22 217 6992
Address: Dept. of Aeronautics and Space Engineering, Tohoku University, Aoba 01, Seidai 980-8579, Japan

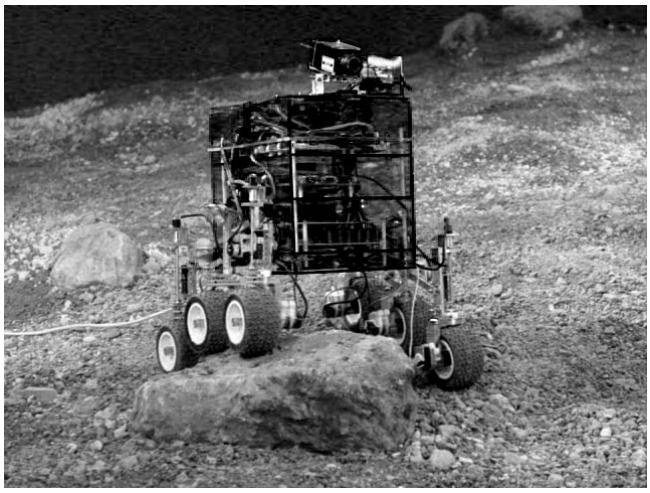

**Figure 1.** A rover test bed "Nexus 6" developed at Tohoku University

We therefore study the traction mechanics of a tire on loose soil, such as dry sand, and derive a model for *load-traction factor*, which is the ratio of the tangent and normal forces on a tire. Here, *slip ratio* of the tire is highlighted as a state variable, and the load-traction factor is derived as a function of the tire slip. The model is verified by experiments.

The motion dynamics of a rover is discussed with the model that a rover's suspension mechanism is treated as an articulated multi-body system connected by a free joint or a differential joint, or a spring-damper mechanism, if necessary. The motion of the rover is simulated using the driving force of the wheels as input.

A traction control method is then developed in order to obtain adequate traction with small slip ratios, avoiding soil failure. In the proposed method, the tire slip is estimated from velocity and the tire torque is controlled to keep the slip ratio within an appropriate level. When the traction force exceeds a maximum share stress of the soil, the soil fails to support the stress and starts to move loosely. If we apply excessive wheel-driving force without noticing such physical behavior of the soil, the wheel will be stuck at a place with digging a hole and sinking in it.

This paper is organized as follows. In section 2, a rover test bed with 6 wheels connected by a Rocker-Bogie type link suspension is introduced. In section 3, the modeling of the rover is discussed for the tire-soil mechanics and the motion dynamics of the vehicle. In section 4, the model is verified by experiments. Characteristic parameters are identified, then the experimentally observed motion is examined by simulation. In Section 5, a control method to achieve higher traversability using slip estimation is proposed and its performance is verified by experiments.

## 2. ROVER TEST BED

The rover test bed developed at Tohoku University, named "Nexus 6," has the dimension of within 0.4 $\times$ 0.4 $\times$ 0.4 [m] cube and weighs 5.8 kg in total (see Figure 1.) It has 6 wheels connected by a Rocker-Bogie type suspension link system. Each wheel, in the diameter of 0.09 [m], is covered by soft rubber surface with small rubber spikes. Front and rear wheels have active steering DOF. The rocker-bogie is a non-spring suspension mechanism to connect wheels by free-pivot links. The mechanism is known as one of successful suspension designs for the traversal capability on rough terrain.[17] The suspension mechanism of our test bed uses parallel links unlike that was used in the Pathfinder rover or other NASA's recent Mars rover prototypes, but its functionality is almost the same. The right and left rocker links are connected by a differential mechanism.

In the main body, compact CPU boards (Hitachi H8) and motor drivers are mounted to control the driving torque of the wheels using pulse width moderation (PWM.) The CPU cards communicate with a host computer through wired (RS-232C) or wireless (Ethernet) connection.

During the operation, duty ratio of the PWM pulse, which is effectively in proportion to the driving torque, is given to the motor driver of each wheel from the host computer as control input. The state of the rover is measured by following sensors: 6 tachogenerators for wheel angular velocity, 4 potentiometers for front and rear steering angles, 4 potentiometers for the suspension link angles (right and left rockers, right and left bogies.) The orientation and traveling velocity of the rover in the inertial frame is measured by a 3D video tracking system. For the tracking, 4 optical cue markers (colored balls) are attached on the test bed.

## 3. MODELING

### 3.1. Slip Ratio

As a key variable to describe the state of the rover, and to perform control, this paper focuses the slip ratio $S$ of each wheel. It is defined as follows:

$$S = \begin{cases} (r\dot{\theta}_w - v_w)/r\dot{\theta}_w & (r\dot{\theta}_w > v_w : \text{accelerating}) \\ \\ (r\dot{\theta}_w - v_w)/v_w & (r\dot{\theta}_w < v_w : \text{braking}) \end{cases} \tag{1}$$

where

$r$ : radius of the wheel
$\theta_w$ : rotation angle of the wheel ($\dot{\theta}_w = \boldsymbol{\omega}$)
$r\dot{\theta}_w$ : tire circumference velocity
$v_w$ : traveling velocity of the wheel

In this definition, the slip ratio is positive when the vehicle is accelerating and negative when braking.

### 3.2. Tire-Soil Interaction Mechanics

Figure 2 depicts a model of a wheel on deformable terrain. For such a model, a formula is known to describe the relationship between the share stress $\tau(\theta)$ and the normal stress $\sigma(\theta)$ of loose soil beneath the wheel[18]:

$$\tau(\theta) = (c + \sigma(\theta)\tan\phi)(1 - \exp[-\frac{r}{k}\{\theta_1 - \theta - (1-S)(\sin\theta_1 - \sin\theta)\}]) \tag{2}$$

where

$$\tau_{max} = c + \sigma\tan\phi \tag{3}$$

represents a maximum share stress of the soil.

Also, another formula for the normal stress to relate the wheel's vertical sinkage $h$ has been proposed[19]:

$$\sigma(h) = (k_1 + k_2 b)(\frac{h}{b})^n \tag{4}$$

where the geometrical relationship for $h$ is:

$$h = r(1 - \cos\theta_1) \tag{5}$$

In the above equations, the symbols are:

$c$ : cohesion stress of the soil
$\phi$ : internal friction angle of the soil

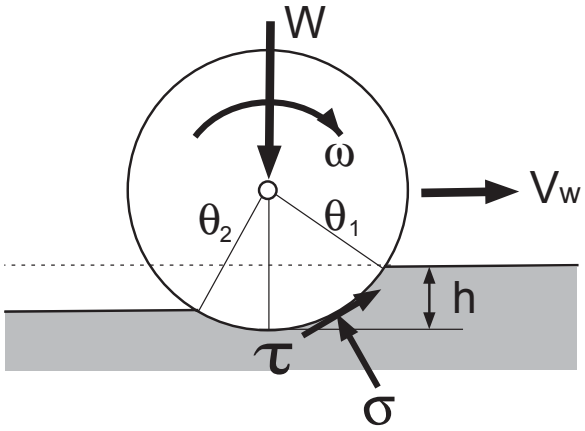


**Figure 2**: A tire model on deformable soil

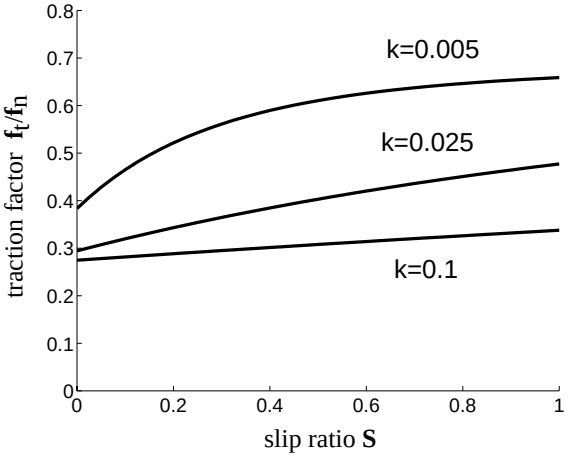


**Figure 3.** Traction factor versus slip ratio for various $k$

$b$ : wheel width
$n, k, k_1, k_2$ : constants

By integrating $\sigma$ and $\tau$ over the entire contact area, from $\theta_2$ to $\theta_1$, we obtain the normal and tangential forces exerting on the wheel:

$$f_n = rb\{\int_{\theta_2}^{\theta_1} \sigma(\theta)\cos\theta d\theta + \int_{\theta_2}^{\theta_1} \tau(\theta)\sin\theta d\theta\} \tag{6}$$

for the normal force that is balanced to the load $W$, and

$$f_t = rb\{\int_{\theta_2}^{\theta_1} \tau(\theta)\cos\theta d\theta - \int_{\theta_2}^{\theta_1} \sigma(\theta)\sin\theta d\theta\} \tag{7}$$

for the tangential force that is called *drawbar pull.*

Here, we are interested in the drawbar pull as a function of the slip ratio. Since it is difficult to obtain a closed form solution of the above equations for the slip $S$, the solutions are examined numerically. By changing $S$ and $k$, while holding other parameters constant at $c = 0.005[\mathrm{N/m}^2], \phi = 30[\mathrm{deg}], \theta_1 = 35[\mathrm{deg}], \theta_2 = -5$ [deg] in equations (2)-(7), we obtain Figure 3. In the figure, the vertical axis indicates the ratio of the traction force (drawbar pull) and normal force, i.e. $F(S) = f_t/f_n$, which is called *load-traction factor.*

The plots of the traction factor versus the slip ratio are displayed for various $k$, which is a constant to represent the share displacement at the maximum share stress and specific to the soil. The value of $k$ will be identified from experimental observation in the following section.

### 3.3. Articulated Body Dynamics

Here, the motion dynamics of the rover is discussed with a model that the rover's suspension mechanism is treated as an articulated multi-body system. Figure 4 depicts the model representing forces and moments exerting on the system. Equation of motion for this system is formulated as follows:

$$\boldsymbol{H}\begin{bmatrix} \dot{\boldsymbol{v}}_0 \\ \dot{\boldsymbol{\omega}}_0 \\ \ddot{\boldsymbol{\theta}}_s \\ \ddot{\boldsymbol{\theta}}_r \\ \ddot{\boldsymbol{\theta}}_w \end{bmatrix} + \boldsymbol{C} = \begin{bmatrix} \boldsymbol{F}_0 \\ \boldsymbol{N}_0 \\ \boldsymbol{n}_s \\ \boldsymbol{n}_r \\ \boldsymbol{n}_w \end{bmatrix} + \boldsymbol{J}^T\boldsymbol{F}_e \tag{8}$$

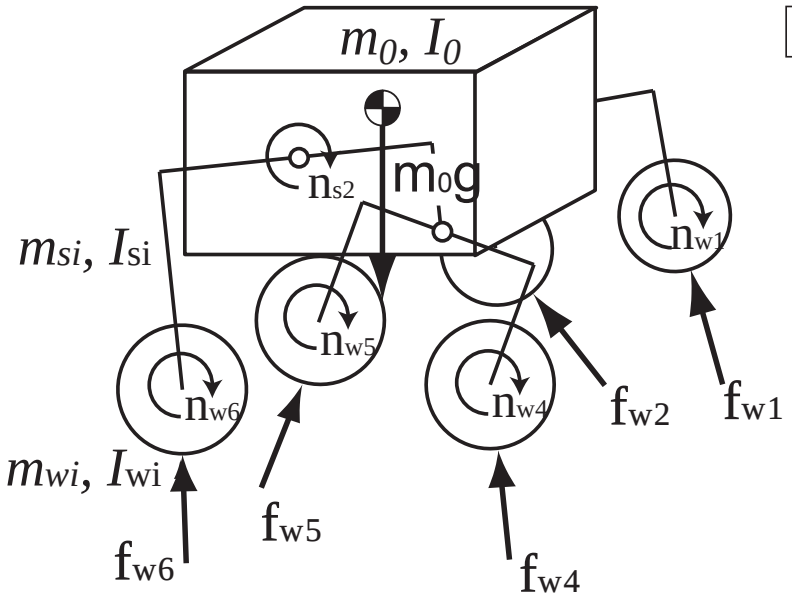


**Figure 4.** An articulated body model of the Rocker-Bogie suspension

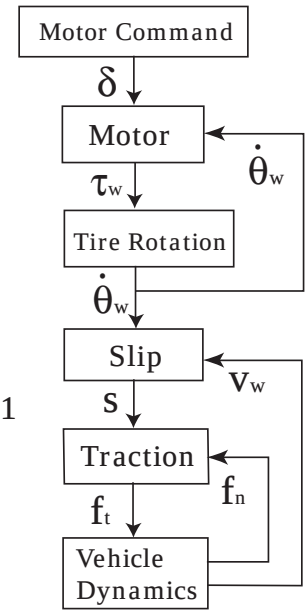


**Figure 5.** A computational flow for the forward dynamics simulation

In this equation, the symbols are:

- $\boldsymbol{H}$ : inertia matrix for the entire system composed by the inertia property of each body
- $\boldsymbol{C}$ : non-linear velocity-dependent term
- $\boldsymbol{v}_0$ : translational velocity of the base body
- $\boldsymbol{\omega}_0$ : rotational velocity of the base body
- $\boldsymbol{\theta}_s$ : suspension angle
- $\boldsymbol{\theta}_r$ : steering angle
- $\boldsymbol{\theta}_w$**:** rotational angle of the wheel
- $\boldsymbol{F}_0 = (0, 0, -m_0 g)^T$: forces exerting on the base body
- $\boldsymbol{N}_0$ : moments exerting on the base body
- $\boldsymbol{n}_s$ : torque on the suspension joints
- $\boldsymbol{n}_r$ : torque on the steering joints
- $\boldsymbol{n}_w$ : driving torque of the wheels
- $\boldsymbol{J}$ : Jacobian matrix
- $\boldsymbol{F}_e = (f_{w1}^T, \cdots, f_{w6}^T)^T$: tire forces

Because of the differential mechanism between the right and left rocker links, there is a kinematic constraint so that $\theta_{s1} = -\theta_{s2}$ (angles are relative to the base body,) and the corresponding constraint torques are considered in $\boldsymbol{N}_0$ and $\boldsymbol{n}_s$.

The driving torque of the wheel is modeled including the characteristics of a PWM controlled DC motor. The tire force component $f_{wi}$ is composed by the normal force $f_{ni}$ and the tangential force $f_{ti}$. Given the sinkage and the slip ratio of each wheel, the normal stress and force are obtained from Equations (4) and (6), respectively. The tangential force is then obtained by multiplying the load-traction factor to the normal force.

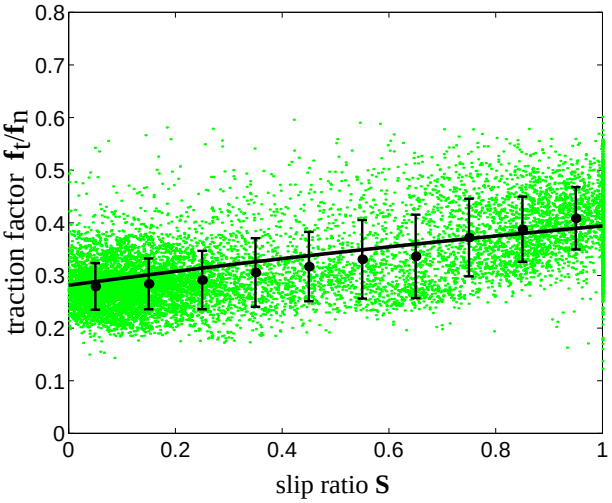


**Figure 6.** Traction factor v.s. slip ratio: experimental plots and a theoretical curve

**Table 1.** Characteristic parameters for the tire-soil interaction identified from experiments

| | | |
|---|---|---|
| $c$ | 0.005 | [N/m$^2$] |
| $\phi$ | 30 | [deg] |
| $k$ | 0.05 | [m] |
| $\theta_1$ | 35.0 | [deg] |
| $\theta_2$ | -5.0 | [deg] |

### 3.4. Forward Dynamics Simulation

The authors have been developing an in-house software, in the form of MATLAB toolbox, for the numerical computations of kinematics and dynamics of articulated body systems. The toolbox is named *SpaceDyn*.[20,21] We use it as a core module to obtain the forward dynamics solution of Equation (8).

The computational flow of the forward dynamics simulation is described in Figure 5. First, the PWM duty ratio $\boldsymbol{\delta}$ is given as control input, then the motor torque is determined with the feedback of the back electromotive force that is a function of the angular velocity of the motor. Second, the slip ratio is evaluated from the velocities of the wheel and vehicle, then the traction forces are obtained using the load-traction factor. Finally, the vehicle dynamics is solved to obtain the acceleration of each part of the rover, then integrated to yield corresponding velocity and position.

The traveling velocity of the wheels is fed back to the slip evaluation. And also, by evaluating the interference of wheels with a surface geometry model, the wheel sinkage is evaluated to determine the normal forces.

By repeating this cycle, the motion of the rover is simulated in the virtual world.

## 4. IDENTIFICATION AND VERIFICATION

In this section, the tire-soil contact model and the dynamics simulation model, discussed in the previous section, are verified by experiments. As for the tire-soil model, specific parameters to describe the load-traction factor are identified. For the dynamics model, the motion profiles are compared between the experiment and simulation.

Experiments are carried out for the rover to traverse over dry sand. The grain of the sand is almost between 0.2 and 2.0 millimeters. The test filed includes a sharp ditch in the depth of 5 centimeters and smooth slopes up to the inclination of 20 degrees. In order to test obstacle negotiation, several rocks with the diameter of 5-10 centimeters are scattered over the sand.

During the experiments, the angular velocity of each wheel and the angles of suspension links are measured on board. The velocity of the rover main body is measured external sensors, including a video tracking system. For the purpose of analysis, the traction force is evaluated from the angular velocity of the wheel using the characteristics of the corresponding motor. The normal load on each tire is evaluated from the body attitude and the suspension link angles considering static balance among forces and moments.

### 4.1. Identification of Tire-Soil Parameters

The load-traction factors for various slip ratios, observed in the experiments, are depicted in Figure 6. The data plots are relatively scattered, then mean values at each slip ratio are depicted with an error bar indicating ±1SD (standard deviation.) It is observed that the plots show an increasing trend according to the slip ratio. The solid line in the figure shows a theoretical curve that makes a best fit with the experimental plots. To obtain the theoretical curve, the specific parameters are used in Equations (2)-(7) as listed in Table 1, where $\phi, c$ and $k$ characterize the soil mechanics and may valid for most of dry sand. For example, in literature it appears that $\phi = 32$ [deg], $c = 0$ and $k = 0.025$ [m].[18]

### 4.2. Verification of the Dynamics Simulation

Here, the results of the dynamics simulation are discussed by comparing with the experimental data.

Figure 7 shows a typical example for the rover to move over an obstacle. The figure compares the snap-shot motion of the rover and the rocker and bogie angles between the experiment and simulation. In the simulation, the same control command are given to the motors as the experiment. It appears that the time scale, which corresponds to the translational velocity of the rover, has difference between the two although, the overall profile shows good agreement. The simulation result well represents the performance of the rocker-bogie suspension system.

The reason of the difference may be inaccuracy of the surface model: i.e. in the simulation, all the surface is modeled as dry sand but, in reality, the obstacle has a hard surface while other flat area is composed by loose sand.

Figure 8 shows a case to negotiate with a slope that has an increasing inclination. In the experiment, the slip ratio stays near 0 before $t = 25$ [s], which means the tire grips the surface without slip. At $t = 25$ [s], the inclination of the slope reaches almost 12 degrees. After that the slip ratio increases up to 1, which means that the tire loses the grip. The elevation stayed constant after $t = 30$ [s] when the slip ratio reached to almost 1, yet the wheel was still driving. At this situation, the tire driving force exceeded the maximum share force of the soil, then the wheel started to dig a hole and sink in it, and finally the rover was stuck.

In the simulation, the time scale (traveling velocity) is again different although, the slip ratio switches from 0 to 1 at the inclination of 12 degrees, same as the experiment. In this sense, the simulation well represents the kinetic motion of a rover traversing over loose soil. However, the elevation keeps rising after switching the value of the slip, because the digging and sinking process is not modeled in the simulation, but Figure 6 suggests the traction force exists even at $S = 1$, which is correct as far as the tire force is lower than the maximum share force of the soil.

## 5. SLIP BASED CONTROL

As suggested in Figure 8, a rover can travel stably when the slip ratio is around 0, but it will be stuck when the slip ratio develops to around 1 and the tangential force exerting to the soil exceeds the maximum share force. Based on this knowledge, we propose a traction control method to target the slip ratio at a small value and to limit the driving torque not to exceed the maximum share.

Figure 9 depicts a block diagram of the proposed control method. In the control, a desired slip value $S_d$ is given as an input command. Then $S_d$ is subtracted by the estimate of the current slip value $\hat{S}$, such that $\Delta S = S_d - \hat{S}$. PI control is composed to regulate the PWM duty ratio $\boldsymbol{\delta}$ to achieve $\Delta S \to 0$. The magnitude of $\boldsymbol{\delta}$ is checked if the resultant torque will exceed the maximum share or not, and limited if it will. For the estimation of the slip, we need the angular velocity and the traveling velocity of the wheel, $\boldsymbol{\omega}$ and $v_w$. The former is easily obtained from the on-board sensor. However the latter is difficult to measure by on-board sensors and an external measurement system will be needed. Here, instead to measure, we estimate the value of $v_w$ from $\boldsymbol{\delta}$ using an empirical function table. For example, we know that our test bed runs at velocity of 0.05 [m/s] in a steady state when $\boldsymbol{\delta} = 0.55$ is given. In this way, the slip is estimated as:

$$\hat{S} = \frac{r\boldsymbol{\omega} - \hat{v}_w(\boldsymbol{\delta})}{r\boldsymbol{\omega}} \tag{9}$$

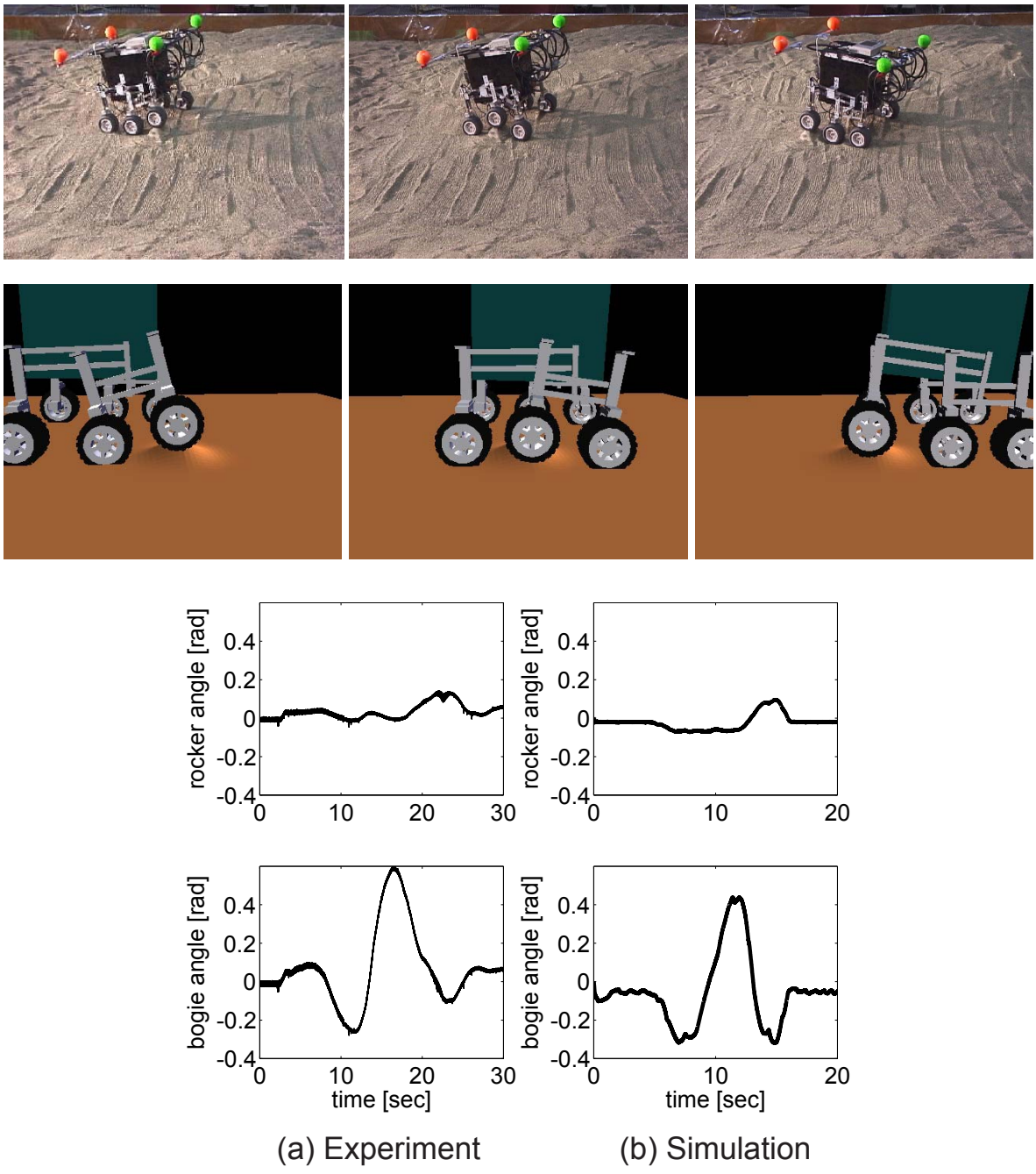


**Figure 7**: Rover motion moving over a bump: comparison of experiment and simulation

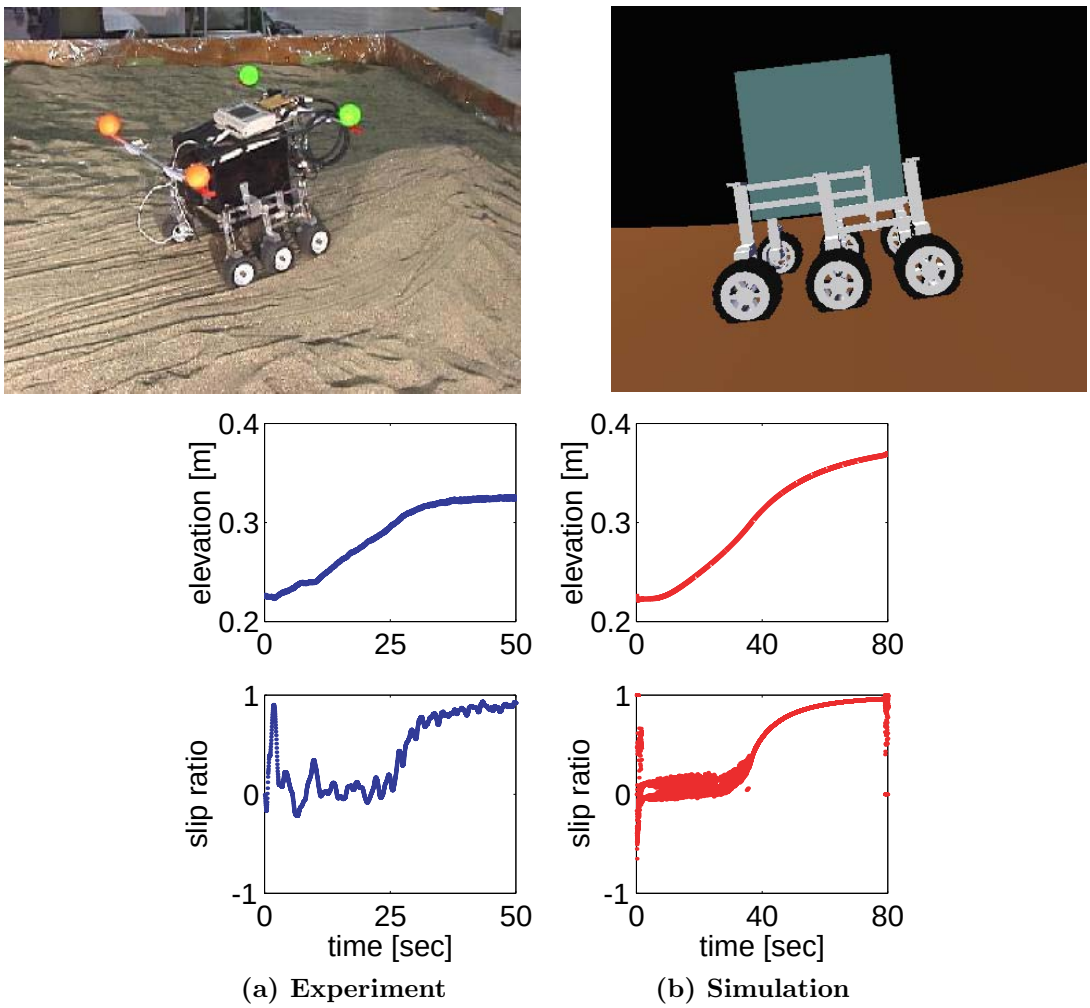


**(a) Experiment** **(b) Simulation**

**Figure 8**: Rover motion to climb up a slope: comparison of experiment and simulation

Experimental comparison between with and without the control is depicted in Figure 10. In the experiments, traversal over a sandy ditch, which has 0.05 [m] depth and 0.2 [m] width, is tested. The left graphs show the case without the slip control and the right graphs show the case with the slip control. Top row draws the real, not the estimation used in the control, slip ratio of the middle wheel. Bottom row draws the traveling velocity of the rover. And the very top of the figure, snap-shots are displayed to illustrate the sequence of the motion (time elapses from left to right, the rover runs from right to left.)

In case with control, $S_d = 0.1$ is given as a control command and each motor torque is regulated independently to realize the control algorithm described in the above. On the other hand, in case without control, a constant PWM duty ratio at $\boldsymbol{\delta} = 0.55$ is given for all six wheels all the time.

As a result, in case without control, the rover was running at $v = 0.05$ [m/s] and $S$ equals to almost 0 for the first 5 seconds, then went down in the ditch. At that moment, the rover velocity increased temporarily. Immediately after that, the front wheel hit the up-edge of the ditch but unsuccessful to climb up, then the vehicle lost the velocity at $t = 7$ [s]. After the vehicle has stopped, the wheel was yet rotating constantly, then the slip ratio went up to $S = 1$ and there was no chance to get recovered.

In case with control, the sequence was almost the same till $t = 7$ [s]. However, when the slip ratio went to $S = 1$ at $t = 8$ [s], the slip control functioned to slow down the wheel velocity. This action worked out

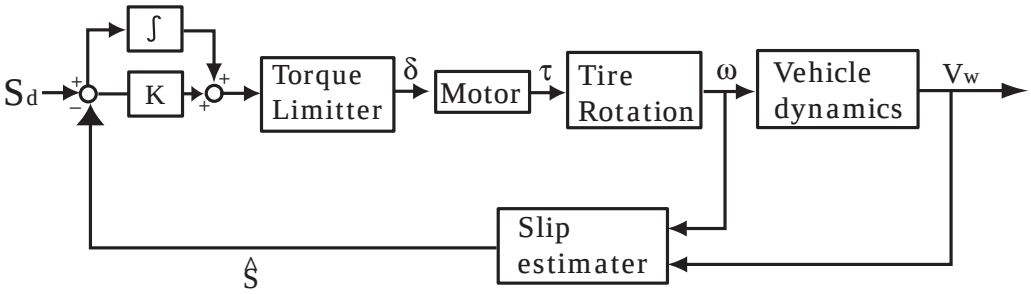


**Figure 9**: A block diagram of the proposed slip-based traction control

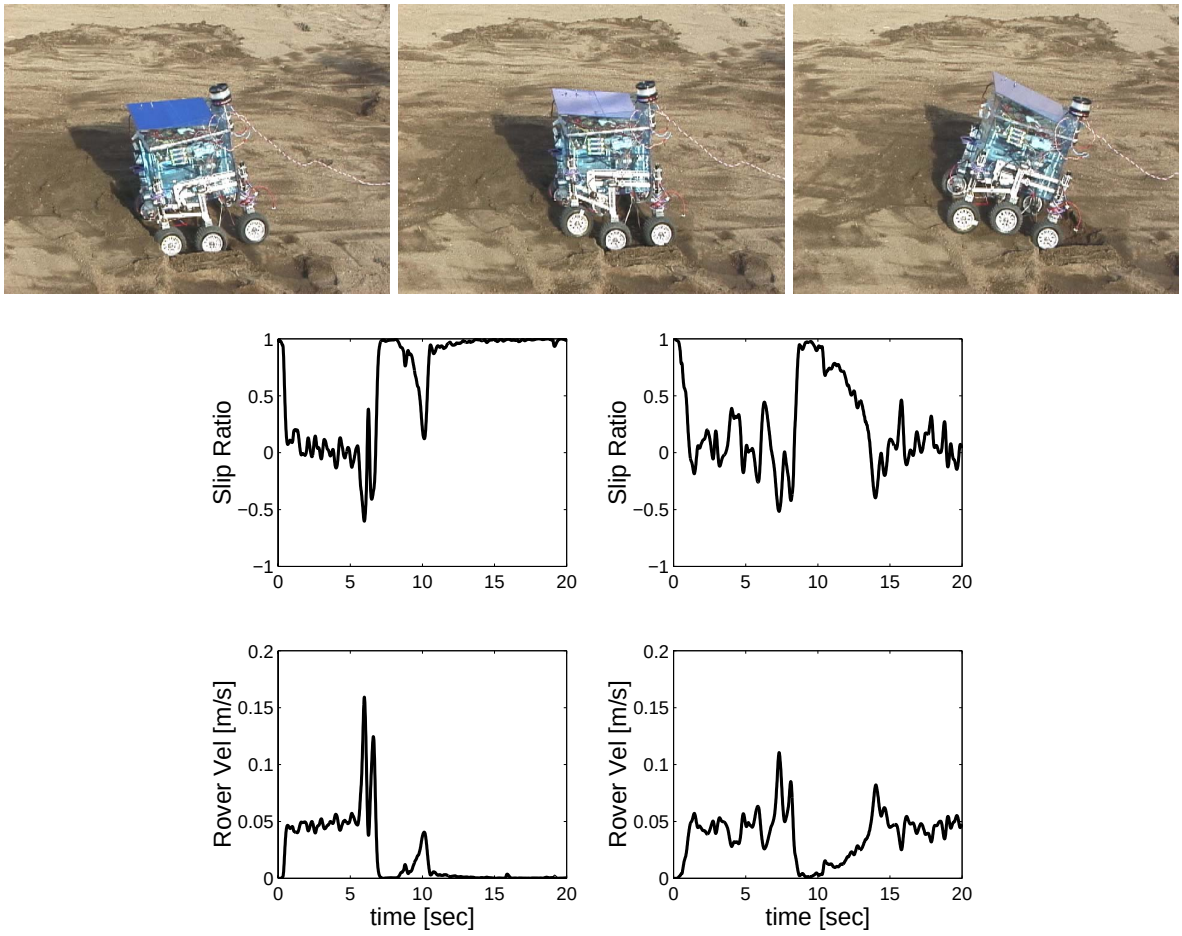


**(a) Without Slip Control** **(b) With Slip Control**

**Figure 10**: Moving over a ditch (depth of 0.05 [m], width of 0.2 [m].) Left: without control, Right: with control

successfully to get the tire slip decreased, as well as the vehicle velocity increased. Finally, after $t = 14$ [s] the rover went out of the ditch, then the steady state that $v = 0.05$ [m/s] and $S$ is at a small positive value was recovered.

## 6. CONCLUSIONS AND FUTURE WORK

In this paper, the authors have investigated the kinetic behavior of a planetary rover with attention to tire-soil traction mechanics and articulated body dynamics, when the rover travels over natural rough terrain. They also have developed an effective control law to increase the traversability paying attention to the slip of the wheels.

Experiments were carried out with a rover test bed to observe the physical phenomena of soils and to model the traction mechanics using the tire slip ratio as a state variable. The relationship of load-traction factor versus the slip ratio has been modeled theoretically then verified by experiments. Specific parameters to characterize the soil have been also identified.

A dynamics simulation model was developed considering the characteristics of a wheel actuator, the mechanics of tire-soil traction, and the articulated body dynamics of a suspension mechanism. Simulations were carried out to compare the corresponding experimental data and verified to represent the physical behavior of the rover.

Finally, a control method has been proposed and tested. The proposed method uses the estimated value of the slip ratio then tries to keep it within a small value and limits excessive tire force, so that the rover can successfully traverse over an obstacle without digging the soil or being stuck. The proposed control method was successfully demonstrated to traverse over a ditch, which was not done without the control.

As a future research, the authors are interested in simulating the rover motion in the smaller gravity environment such as on the Moon or the Mars, where the dynamic effect will be much more highlighted.


### Acknowledgements

A part of the experiments were carried out at the Robotics Laboratory in Tsukuba Space Center, NASDA, Japan. The research is supported by the Ministry of Education, Science, Sports and Culture, Grant-in-Aid for Scientific Research (B), 10044113, 1998-2001.


## REFERENCES


1. http://mars.jpl.nasa.gov/MPF/ (as of Feb. 2002)
2. http://mars.jpl.nasa.gov/mep/missions/announce2.html (as of Feb. 2002)
3. C.R.Weisbin, D.Lavery, G.Rodriguez; "Robotics Technology for Planetary Missions Into the 21st Century," *Proc. i-SAIRAS'97,* Tokyo, Japan, July, 1997, pp.5–10.
4. C.R.Weisbin,et. al.; "Autonomous Rover Technology for Mars Sample Return," *Proc. i-SAIRAS'99,* ESTEC, The Netherlands, June, 1999, pp.1–10.
5. Paolo Fiorini; "Ground Mobility Systems for Planetary Exploration," *Proc. 2000 IEEE Int. Conf. of Robotics and Automation,* CA, USA, April, 2000, pp.908–913.
6. J.Aizawa, N.Yoshioka, M.Miyata, Y.Wakabayashi; "Designing of Lunar Rovers for High Work Performance," *Proc. i-SAIRAS'99,* ESTEC, The Netherlands, June, 1999, pp.63–68.
7. Y.Kuroda, K.KOndo, K.Nakamura, Y.Kunii, T.Kubota; "Low Power Mobility System for Micro Planetary Rover *Micro5*," *Proc. i-SAIRAS'99,* ESTEC, The Netherlands, June, 1999, pp.77–82.
8. M.Tarokh, Z.Shiller, S.Hayati; "A Comparison of Two Traversability Based Path Planners for Planetary Rovers," *Proc. i-SAIRAS'99,* ESTEC, The Netherlands, June, 1999, pp.151–157.
9. J. Balaram; "Kinematic Observers for Articulated Rovers," *Proc. 2000 IEEE Int. Conf. of Robotics and Automation,* CA, USA, April, 2000, pp.2597–2604.
10. S.Hayati, R.Arvidson; "Long Range Science Rover (Rocky7) Mojave Desert Field Tests," *Proc. i-SAIRAS'97,* Tokyo, Japan, July, 1997, pp.361–367.

11. W.R.Whittaker, D.Bapna, M.W.Maimone, E.Rollins; "Atacama Desert Trek: A Planetary Analog Filed Experiment." *Proc. i-SAIRAS'97,* Tokyo, Japan, July, 1997, pp.355–360.
12. Farritor, S., Hacot, H., and Dubowsky, S.;gPhysics-Based Planning for Planetary Exploration,h Proceedings of the 1998 IEEE International Conference on Robotics and Automation: 278-283, 1998.
13. Iagnemma, K., Burn, R., Wilhelm, E., and Dubowsky, S.; gExperimental Validation of Physics-Based Planning and Control Algorithms for Planetary Robotic Rovers,hProc. of the Sixth International Symposium on Experimental Robotics, ISER '99, 1999.
14. Iagnemma, K., and Dubowsky, S.; gVehicle Wheel-Ground Contact Angle Estimation: with Application to Mobile Robot Traction Control,h Proc. 7th International Symposium on Advances in Robot Kinematics, ARK 00, 2000.
15. Iagnemma, K., and Dubowsky, S., "Mobile Robot Rough-Terrain Control (RTC) for Planetary Exploration," Proceedings of the 26th ASME Biennial Mechanisms and Robotics Conference, DETC 2000.
16. http://yyy.tksc.nasda.go.jp/sat/selene/index_e.html
http://www.isas.ac.jp/e/enterp/missions/selene/ (as of Feb. 2002)
17. Bickler, D., "A New Family of JPL Planetary Surface Vehicles," Missions, Technologies, and Design of Planetary Mobile Vehicles, pp. 301-306, 1992.
18. Wong, J. Y., Theory of Ground Vehicles, John Wiley & Sons, 1978, chapter 2.
19. Bekker, G., Introduction to Terrain-Vehicle Systems, University of Michigan Press, 1969.
20. K. Yoshida; "The SpaceDyn: a MATLAB Toolbox for Space and Mobile Robots," J. of Robotics and Mechatronics, vol.12 no.4, pp.411–416, 2000.
21. http://www.astro.mech.tohoku.ac.jp/spacedyn